An Improved Algorithm for Through-Wall Target Detection Using Ultra-Wideband Impulse Radar

Xiaolin Liang, Hao Zhang, Guangyou Fang, Shengbo Ye, and T. Aaron Gulliver

2017

IEEE Access
Multidisciplinary | Rapid Review | Open Access Journal

Received September 6, 2017, accepted September 29, 2017, date of publication October 10, 2017,
date of current version November 7, 2017.

Digital Object Identifier 10.1109/ACCESS.2017.2761771

An Improved Algorithm for Through-Wall Target Detection Using Ultra-Wideband Impulse Radar

XIAOLIN LIANG[1,2], HAO ZHANG[1,3], (Senior Member, IEEE), GUANGYOU FANG[2], SHENGBO YE[2], AND T. AARON GULLIVER[3], (Senior Member, IEEE)

[1]Department of Electronic Engineering, Ocean University of China, Qingdao 266100, China
[2]Key Laboratory of Electromagnetic Radiation and Sensing Technology, Institute of Electronics, Chinese Academy of Sciences, Beijing 100190, China
[3]Department of Electrical and Computer Engineering, University of Victoria, Victoria, BC V8W 2Y2, Canada

Corresponding author: Xiaolin Liang (e-mail: iamxiaolin2016@126.com)

This work was supported in part by the Nature Science Foundation of China under Grant 41527901, in part by the Major Program of China's Second Generation Satellite Navigation System under Grant GF**********03, in part by the Fundamental Research Funds for the Central Universities under Grant 201713018, in part by the National High Technology Research and Development Program of China under Grant 2012AA061403, in part by the National Science and Technology Pillar Program during the Twelfth Five-year Plan Period under Grant 2014BAK12B00, and in part by the National Natural Science Foundation of China under Grant 61501424.

ABSTRACT This paper considers the detection and localization of a human subject in complex environments using an ultra-wideband impulse radar. The subject is remotely sensed by extracting micro-motion information, such as the respiration and heartbeat frequencies. It is challenging to extract this information due to the low signal to noise and clutter ratio in typical disaster environments. To improve the localization accuracy, a new method is proposed using the characteristics of vital sign signals. The range is determined using a short-time Fourier transform of the kurtosis and standard deviation of the received signals. Furthermore, an improved arctangent demodulation technique is used to determine the frequency of human micro-motion based on a multiple frequency accumulation method. Performance results are presented, which show that the proposed method is superior to several well-known techniques.

INDEX TERMS Human micro-motion, ultra-wideband (UWB) impulse radar, short-time Fourier transform (STFT), kurtosis, frequency accumulation (FA), arctangent demodulation (AD).

I. INTRODUCTION

Radar can be used to detect human targets by sensing body surface motion caused by respiration and heartbeat [1]–[5]. Two classes of radar have been used for this purpose, narrowband continuous wave and ultra-wide band (UWB), but UWB radar has better performance in penetrating obstacles and identifying targets [6]–[13]. UWB impulse radar has been the subject of significant research because of its simple structure, low-cost, and low-power consumption. It can remotely detect human vital signs (e.g., respiration and heartbeat), which is useful for medical diagnosis and monitoring. In medical imaging applications, a high center frequency and large bandwidth are employed to provide fine resolution for human tissues and organs. A promising application of this technology is the detection of trapped victims during post-disaster search and rescue. This requires not only good penetration but also sufficient sensitivity to detect the vital signs of trapped victims, who are usually otherwise motionless. This can be achieved by using a lower center frequency and detecting victims by their respiration and/or heartbeat [14]–[22].

Several vital sign detection algorithms have been proposed [23]–[40]. However, many of these approaches are not suitable after a natural disaster, as they deal with only some aspects of the environment such as removing static and non-static clutter, detecting human respiration characteristics, or heart rate estimation. The fast Fourier transform (FFT) and Hilbert-Huang transform (HHT) have been employed to analyze the time-frequency characteristics of human respiration [23], [24]. A dual frequency model was developed and the respiration-like clutter removed using adaptive clutter cancellation [8]. In [27], a low complexity maximum likelihood (ML) estimation method was proposed to estimate the human respiration period in additive white Gaussian noise (AWGN) [27]. In [28], singular value decomposition (SVD) was employed to extract human respiration information in low signal to noise and clutter ratio (SNCR) conditions.

In [33], a tracing method was employed to detect signs of life, but it is effective only over short distances with a high signal to noise ratio (SNR). The static clutter was removed using linear trend subtraction (LTS) in [28]. In [35], higher order cumulants (HOCs) were used to extract vital sign information by exploiting the fact that the HOCs of Gaussian noise are zero. Although this approach was designed for Gaussian noise environments, it can significantly improve vital sign detection in other types of noise. In [36], ensemble empirical mode decomposition (EEMD) was used to analyze variations in the human heart rate. In [37], complex signal demodulation (CSD) was proposed to remove clutter. Vital signs were extracted using a state space method (SSM) in [39], but this approach is effective only over short distances.

It is difficult to accurately extract vital signs such as the human respiration frequency and heart rate using existing methods due to the complexity of the signal analysis and the significant memory requirements. Further, these methods are only suitable for short distances with a high SNCR. In this paper, an effective method is proposed to accurately detect trapped victims even in low SNCR environments such as in long range and through-wall conditions. Localization is achieved using the short-time Fourier transform (STFT) of the kurtosis and standard deviation of the received signal. Further, an improved arctangent demodulation (AD) technique is presented to estimate human micro-motion frequencies based on a multiple frequency accumulation (FA) method. The trapped victim is then identified in a distance-frequency matrix. The performance of this method is compared with several well-known algorithms using the UWB radar designed by the Key Laboratory of Electromagnetic Radiation and Sensing Technology, Institute of Electronics, Chinese Academy of Sciences.

The remainder of this paper is organized as follows. In Section II, the system model is given, and the proposed method for range and vital sign detection is presented in Section III. In Section IV, the performance of this method is evaluated and compared with several well-known techniques. Finally, Section V concludes the paper.

II. VITAL SIGN MODEL

A. SYSTEM MODEL

In this section, the model for human target detection, and the respiration and heartbeat frequencies are presented. With the UWB impulse radar, the subject can be detected from changes in the propagation delay of the received signal. The distance from the antenna to the subject is given by [32], [35]

$$d(t) = d_0 + r(t) = d_0 + A_r \sin(2\pi f_r t) + A_h \sin(2\pi f_h t) \quad (1)$$

where d_0 is the nominal distance between the antenna and human chest, A_r is the respiration displacement amplitude, f_r is the respiration frequency, A_h is the heartbeat displacement amplitude, and f_h is the heartbeat frequency. Assuming only one subject exists in the detection environment, all other objects are stationary. The impulse response is then

$$h(\tau, t) = a_v \delta(\tau - \tau_v(t)) + \sum_i a_i \delta(\tau - \tau_i) \quad (2)$$

where τ is the propagation time and $\sum_i a_i \delta(\tau - \tau_i)$ denotes the response from the ith static target with amplitude a_i, and $a_v \delta(\tau - \tau_v(t))$ denotes the response due to human micro-motion with propagation time $\tau_v(t)$ and amplitude a_v. The propagation time $\tau_v(t)$ is given by

$$\tau_v(t) = \frac{2d(t)}{v} = \tau_0 + \tau_r \sin(2\pi f_r t) + \tau_h \sin(2\pi f_h t) \quad (3)$$

where $v = 3 \times 10^8$ m/s is the speed of light, $\tau_r = 2A_r/v$ and $\tau_h = 2A_h/v$.

The received radar signal can be expressed as

$$R(\tau, t) = s(\tau) * h(t, \tau) = a_v s(\tau - \tau_v(t)) + \sum_i a_i s(\tau - \tau_i) \quad (4)$$

where $s(\tau)$ is the transmitted signal and $*$ denotes convolution.

Equation (4) can be expressed in discrete form as

$$\begin{aligned} R[m, n] &= a_v s(m\delta_T - \tau_v(nT_s)) + \sum_i a_i s(m\delta_T - \tau_i) \\ &= a_v s(m\delta_R - v\tau_v(nT_s)) + \sum_i a_i s(m\delta_R - v\tau_i/2) \\ &= h[m, n] + c[m] \end{aligned} \quad (5)$$

where T_s is the pulse duration, N is the number of samples in slow time, δ_T is the fast time sampling interval, M is the number of fast time samples, and $\delta_R = v\delta_T/2$. The discrete human micro-motion signal is $h[m, n]$ and the static clutter is $c[m]$ which can be considered as a slow time-invariant signal.

To illustrate fast and slow time, Figure 1 shows the received signal due to human respiratory motion. The dashed line denotes a fast time bin. To avoid range ambiguities and frequency aliasing, T_s must be chosen so that all signals from

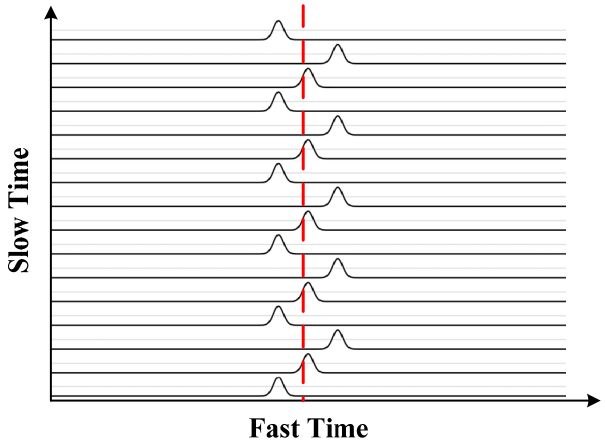

FIGURE 1. The received signal due to human respiration.

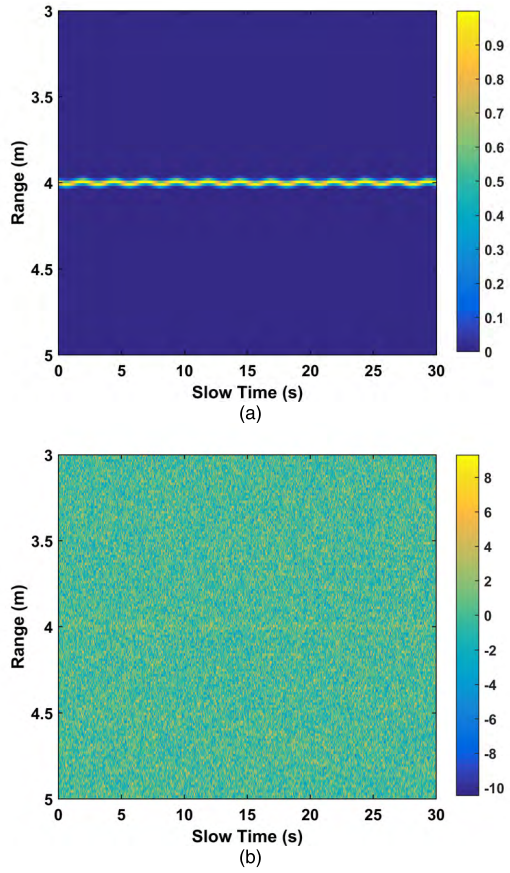

FIGURE 2. The resulting matrix (a) without clutter and (b) with AWGN.

the objects are received in one pulse repetition time and to satisfy the Nyquist sampling theorem, which gives

$$1/T_s \geq 2\left(\max\left(f_r, f_h\right)\right) \tag{6}$$

and

$$T_w + \max\left\{\tau_v\left(t\right)\right\} - \min\left\{\tau_v\left(t\right)\right\} < T_s \tag{7}$$

where T_w corresponds to the -6 dB bandwidth.

Significant clutter can exist in the detection environment. In addition, linear trend, Gaussian noise, non-static clutter, and other clutter can exist in the received signal. In this case, the received signal can be expressed as

$$R\left[m,n\right] = h\left[m,n\right] + c\left[m\right] + a\left[m,n\right] + w\left[m,n\right] + q\left[m,n\right] + g\left[m,n\right] \tag{8}$$

where $a\left[m,n\right]$ represents the linear trend due to the radar triggering, $w\left[m,n\right]$ is AWGN, $q\left[m,n\right]$ is the non-static clutter, and $g\left[m,n\right]$ denotes any other clutter.

Figure 2(a) presents an ideal received signal matrix which contains only the human micro-motion, while the corresponding matrix with only AWGN is given in Figure 2(b). This shows that it is difficult to extract vital sign signals in a low SNR environment. The static clutter is slow time independent and so can be removed by subtracting the average of $R\left(\tau, t\right)$ to obtain $\widetilde{R}\left(\tau, t\right)$ which from (4) can be expressed as

$$\widetilde{R}\left(\tau, t\right) = a_v s\left(\tau - \tau_v\left(t\right)\right) \tag{9}$$

B. SIGNAL DETECTION

To obtain f_r and f_h, the Fourier transform (FT) of $\widetilde{R}\left(m\delta_T, t\right)$ is taken in each slow time dimension which gives

$$Y_m\left(f\right) = \int_{-\infty}^{+\infty} \widetilde{R}\left(\mathrm{m}\delta_T, t\right) e^{-j2\pi ft}\, dt \tag{10}$$

Expressing this in two dimensions we have

$$Y\left(\mathrm{m}\delta_T, f\right) = \int_{-\infty}^{+\infty} Y\left(\upsilon, f\right) e^{j2\pi\upsilon\tau}\, d\upsilon \tag{11}$$

$$Y\left(\upsilon, f\right) = \int_{-\infty}^{+\infty}\int_{-\infty}^{+\infty} \widetilde{R}\left(\mathrm{m}\delta_T, t\right) e^{-j2\pi ft} e^{-j2\pi\upsilon\tau}\, dt d\tau \tag{12}$$

$$\begin{aligned} Y\left(\upsilon, f\right) &= \int_{-\infty}^{+\infty} a_v S\left(\upsilon\right) e^{-j2\pi ft} e^{-j2\pi\upsilon\tau_v(t)}\, dt \\ &= a_v S\left(\upsilon\right) e^{-j2\pi\upsilon\tau_0} \int_{-\infty}^{+\infty} \\ &\quad \times e^{-j2\pi\upsilon m_b \sin(2\pi f_r t)} e^{-j2\pi\upsilon m_h \sin(2\pi f_h t)} e^{-j2\pi ft}\, dt \end{aligned} \tag{13}$$

where $S\left(\upsilon\right)$ is the FT of the received signal in fast time. Then

$$\begin{aligned} Y\left(\upsilon, f\right) &= a_v S\left(\upsilon\right) e^{-j2\pi\upsilon\tau_0} \\ &\quad \times \int_{-\infty}^{+\infty} \left(\sum_{k=-\infty}^{+\infty} J_k\left(\beta_r\upsilon\right) e^{-j2\pi kf_r t}\right) \\ &\quad \times \left(\sum_{l=-\infty}^{+\infty} J_l\left(\beta_h\upsilon\right) e^{-j2\pi lf_h t}\right) e^{-j2\pi ft}\, dt \end{aligned} \tag{14}$$

where

$$e^{-jz\sin(2\pi f_0 t)} = \sum_{k=-\infty}^{+\infty} J_k\left(z\right) e^{-j2\pi kf_0 t} \tag{15}$$

with $\beta_r = 2\pi A_r$ and $\beta_h = 2\pi A_h$. Equation (10) can be expressed as

$$Y\left(m\delta_T, f\right) = a_v \sum_{k=-\infty}^{+\infty}\sum_{l=-\infty}^{+\infty} G_{kl}\left(\tau\right)\delta\left(f - kf_r - lf_h\right) \tag{16}$$

where

$$G_{kl}\left(\tau\right) = \int_{-\infty}^{+\infty} S\left(\upsilon\right) J_k\left(\beta_r\upsilon\right) J_l\left(\beta_h\upsilon\right) e^{j2\pi\upsilon(\tau-\tau_0)}\, d\upsilon \tag{17}$$

The maximum value $\left|G_{kl}\left(\tau\right)\right|$ is obtained when $m\delta_T = \tau_0$ which is

$$C_{kl} = G_{kl}\left(\tau_0\right) = \int_{-\infty}^{+\infty} S\left(\upsilon\right) J_k\left(\beta_r\upsilon\right) J_l\left(\beta_h\upsilon\right) d\upsilon \tag{18}$$

From

$$Y(\tau_0, f) = a_v \sum_{k=-\infty}^{+\infty} \sum_{l=-\infty}^{+\infty} C_{kl}\delta(f - kf_r - lf_h) \quad (19)$$

the human respiration signal can be obtained by setting $l = 0$ giving

$$C_{k0} = \int_{-\infty}^{+\infty} S(\upsilon) J_k(\beta_r \upsilon) J_0(\beta_h \upsilon) d\upsilon \quad (20)$$

For $\beta_r f_c \ll 1$, where f_c is the center frequency of the signal, we have

$$C_{k0} \approx \int_{-\infty}^{+\infty} S(\upsilon) J_k(\beta_r \upsilon) d\upsilon \quad (21)$$

The heartbeat signal can be obtained by setting $k = 0$ as

$$C_{0l} = \int_{-\infty}^{+\infty} S(\upsilon) J_0(\beta_b \upsilon) J_l(\beta_h \upsilon) d\upsilon \approx \int_{-\infty}^{+\infty} S(\upsilon) J_l(\beta_h \upsilon) d\upsilon \quad (22)$$

and when $\beta_h f_c \ll 1$

$$C_{0l} \approx \int_{-\infty}^{+\infty} S(\upsilon) J_l(\beta_h \upsilon) d\upsilon \quad (23)$$

The above computations can be done in discrete time by sampling the received signal and using an FFT [39]. However, the complexity of this approach is high. Therefore, an improved AD method is presented for range estimation in the next section.

C. ULTRA-WIDE BAND IMPULSE RADAR

The UWB impulse radar used in this paper for data acquisition was constructed by the Key Laboratory of Electromagnetic Radiation and Sensing Technology, Chinese Academy of Sciences. This radar contains two antennas in a $.45 \times .22 \times .45$ m^3 box and is operated via a wireless personal digital assistant (PDA). Table 1 shows the radar parameters used for data acquisition. It operates at a center frequency of 400 MHz with a pulse repetition frequency (PRF) of 600 kHz. The datasets were obtained simultaneously by six segments with a segment time window of 124 ns and $M_s = 682$ samples per segment. The number of samples in fast time is $M = 4092$. To improve the SNR, N_A samples were averaged during data acquisition, so the pulse signals are saved every $M_s N_A/\text{PRF} = 0.0341$ s. In slow time, $N = 512$ pulses are received every 17.6 s. A hybrid sampling scheme combining equivalent-time sampling [41] and real-time [42] sampling was implemented as it outperforms an analog receiver employing only equivalent-time sampling.

Figure 3 gives the two-dimensional (slow time and range) matrix R obtained using the UWB radar with one male human subject at a distance of 7 m from the antenna in an indoor detection environment. This environment will be described in detail in Section IV. The vital sign signals are not noticeable due to the significant signal attenuation in long range and through-wall conditions. This indicates that it is challenging to extract these signals in realistic environments. Therefore, a new method for vital sign detection is developed in the next section.

TABLE 1. Parameters of the UWB impulse radar.

Parameter	VALUE
center frequency	400 MHz
transmitted signal amplitude	50 V
Pulse Repeat Frequency (PRF)	600 KHz
number of averaged values (N_A)	30
time window	124 ns
number of samples (M)	4092
input bandwidth of the Analog to Digital Converter (ADC)	2.3 GHz
ADC sampling rate	500 MHz
ADC sample size	12 bits
receiver dynamic range	72 dB

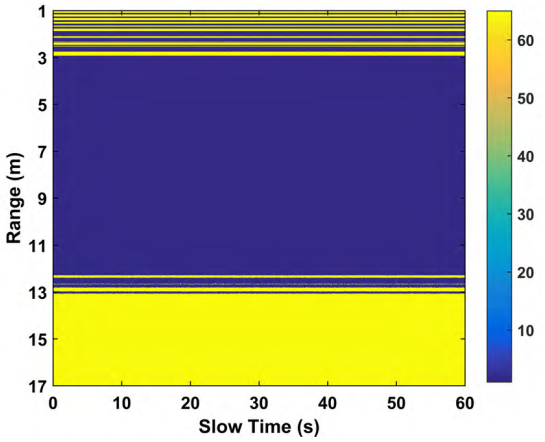

FIGURE 3. The received signal using the UWB radar.

III. PROPOSED METHOD

In this section, the proposed method for signal detection and analysis is presented

A. CLUTTER SUPPRESSION

The static clutter $c[m]$ is usually slow time independent with a large amplitude. The best estimate of the static clutter in the range dimension is obtained by averaging the received values in R as

$$\Im = \frac{1}{M \times N} \sum_{m=1}^{M} \sum_{n=1}^{N} R[m, n] \quad (24)$$

and after subtraction gives

$$\Omega[m, n] = R[m, n] - \Im \quad (25)$$

The LTS method is then used to estimate the DC component and linear trend $a[m, n]$ in the slow time dimension in

$\Omega[m, n]$ using a linear least-squares fit which results in

$$W = \Omega^{\mathrm{T}} - X\left(X^{\mathrm{T}}X\right)^{-1}X^{\mathrm{T}}\Omega^{T} \tag{26}$$

where $X = [x_1, x_2]$, $x_1 = [0, 1, \ldots, N-1]^{\mathrm{T}}$, $x_2 = [1, 1, \ldots, 1]_N^{\mathrm{T}}$, and superscript T denotes transpose.

The received signal depends on the radar characteristics, detection environment, and azimuth between the human target and antenna, as well as the humidity, dielectric constant, and polarization of obstacles. However, these parameters cannot all be predicted accurately, so a matched filter is not a good choice for signal detection. An alternative solution is to use a bandpass filter (BPF) to extract the desired signal such as a Butterworth filter which has transfer function

$$|H(\omega)|^2 = \frac{1}{1 + (\omega/\omega_c)^{2N_f}} \tag{27}$$

where ω_c is the cutoff frequency and N_f is the filter order. The filter performance can be improved by increasing the order, but $N_f = 5$ provides a good tradeoff between performance and complexity. Thus, two fifth-order Butterworth digital filters are employed, a low-pass filter with normalized cutoff frequency 0.1037, and a high-pass filter with normalized cutoff frequency 0.0222. For each slow time index n in W, the filter output is

$$\begin{aligned} &T[m, n] \\ &= \chi_1 W[m, n] + \chi_2 W[m-1, n] + \ldots + \chi_{N_b+1} W[m - N_b, n] \\ &\quad - \kappa_2 W[m-1, n] - \ldots - \kappa_{N_a+1} W[m - N_a, n] \end{aligned} \tag{28}$$

where $N_b = N_a = 5$, and the filter coefficients are κ_i and χ_i.

To further improve the SNR, a smoothing filter is used which has output

$$G[k, n] = \frac{1}{\lambda}\sum_{m=\lambda k}^{\lambda(k+1)-1} T[m, n] \tag{29}$$

where $k = 1, \ldots, \lfloor M/\lambda \rfloor$, $\lfloor M/\lambda \rfloor$ is the largest integer less than M/λ, and $\lambda = 7$. Values of $T[m, n]$ for $m > \lfloor M/\lambda \rfloor$ are set to zero. These filters remove high and low-frequency clutter which improves the SNR.

In reasonably high SNR conditions and in the absence of non-stationary clutter, the response from a breathing victim can be used for range estimation. However, it has been observed from field trials that some of the energy of $q[m, n]$ is likely to appear in R along with the respiration signal, which reduces the detection accuracy. Thus, the goal of the final stage of the algorithm is to reduce the noise and elements of $q[m, n]$ which were not removed during the previous stages, while retaining the desired signal. For this, singular value decomposition (SVD) is used to decompose G into a set of orthonormal matrices which is given by

$$G = U\Sigma V^{T} = \sum_{i=1}^{N} u_i \sigma_{ii} v_i^{\mathrm{H}} \tag{30}$$

where superscript H denotes complex conjugate transpose. The matrix $U = [u_1, u_2, \ldots, u_M]$, $U \in \mathrm{C}^{M\times M}$, is a unitary matrix. The columns of U are called left singular vectors, $u_k \in \mathrm{C}^{M}$, and form an orthonormal basis in slow time so that $u_i \cdot u_j = 1$ for $i = j$ and $u_i \cdot u_j = 0$ otherwise. The matrix $V = [v_1, v_2, \ldots, v_N]$, $V \in \mathrm{C}^{N\times N}$, is also unitary. The rows of V^{H} are the right singular vectors v_n, and also form an orthonormal basis. The matrix $\Sigma \in \Psi_{M\times N}$ has non-zero values $\sigma_{ii} \in \{\sigma_{11} \geq \sigma_{22} \geq \ldots \geq \sigma_{NN}\}$ on the diagonal. Since there are N degrees of freedom in G, $\mathrm{rank}(G) = N$. The components of $q[m, n]$ in G reduces the SNR. It has been shown that this can be suppressed by removing the largest values σ_{ii}, $i = 1, \ldots, n < N$ [28], which gives

$$\Phi = U\Sigma V^{\mathrm{T}} = \sum_{i=n}^{N} u_i \sigma_{ii} v_i^{\mathrm{T}} \tag{31}$$

Using (24) and (31), the static clutter, linear trend, and other clutter in frequencies other than the desired signal can be suppressed. The non-static clutter can be suppressed by ensuring there are no moving objects such as people in the detection environment. The received signal can then be expressed as

$$\Phi(\tau, t) = s(\tau) * h_{target}(t, \tau) = a_v s(\tau - \tau_v(t)) \tag{32}$$

where $h_{target}(t, \tau)$ is the response due to human micro-motion. This can be expressed in discrete form as

$$\Phi[m, n] = a_v s(m\delta_T - \tau_v(nT_s)) = h[m, n] \tag{33}$$

B. RANGE DETERMINATION

In this section, the range is estimated using the statistical characteristic of the received signal. In particular, the standard deviation and kurtosis are used to determine the characteristics of (32) [43], [44]. For each fast time index m in $\Phi[m, n]$, the kurtosis is

$$Kurt = \frac{\mathrm{E}\left[(\Phi[m, n])^4\right]}{\left\{\mathrm{E}\left[(\Phi[m, n])^2\right]\right\}^2} \tag{34}$$

where E[·] denotes expectation. The kurtosis is three for a Gaussian distribution, so the excess kurtosis is typically employed which is given by

$$\widetilde{K} = Kurt - 3 \tag{35}$$

The excess kurtosis is considered here and is denoted as kurtosis in the remainder of the paper. For each fast time index m in $\Phi[m, n]$, the standard deviation is

$$SD = \sqrt{\frac{\sum_{n=1}^{N}(\Phi[m, n] - \mu)^2}{N-1}} \tag{36}$$

where μ is the mean of $\Phi[m, n]$ for the given value of m.

To analyze the signal characteristics, a dataset was acquired indoor with a male subject as the target. The distance between the antenna and target was 7 m in through-wall conditions, with a wall 1 m thick. The experimental setup is discussed in Section IV. The ratio of the standard deviation to

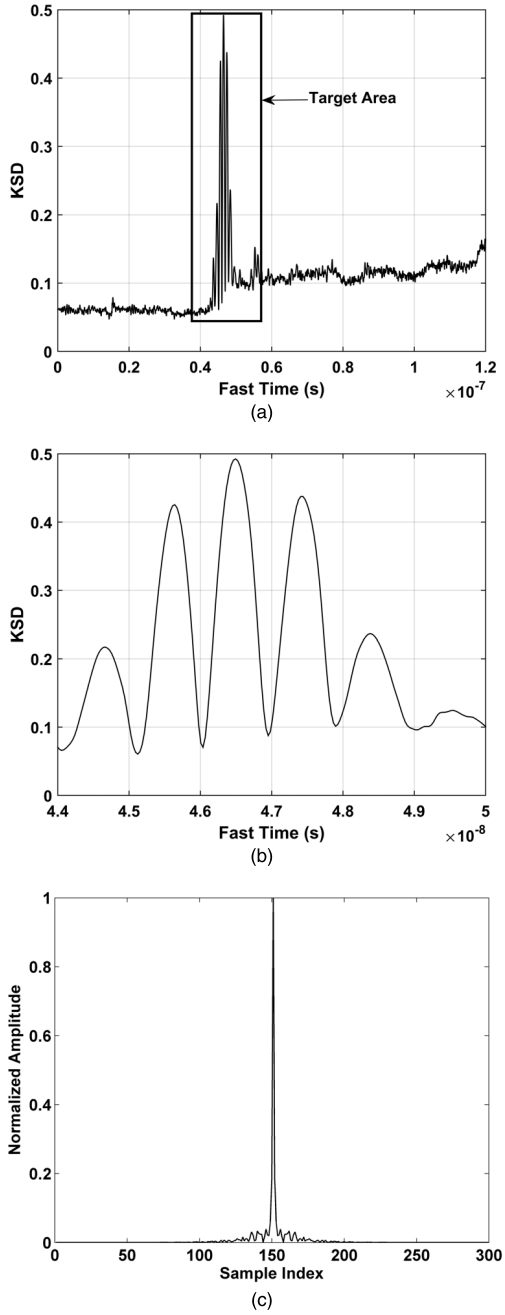

FIGURE 4. The ratio of standard deviation to kurtosis (KSD) using a data set at a distance of 7 m between the human subject and antenna: (a) KSD in fast time, (b) KSD in the target area, and (c) the normalized FFT of the signal in (b).

kurtosis (KSD) $\widehat{\Psi}$, is shown in Figure 4(a). It can be seen that the KSD of the desired signal in the target area is much larger than elsewhere. Figures 4(b) and 4(c) show the KSD in the target area and the corresponding normalized FFT, respectively. This indicates that the signal in the target area is periodic. Figure 5 shows the KSD when a human target is not present. In this case, the result is more uniform with smaller amplitudes and little periodicity compared with Figure 4(b).

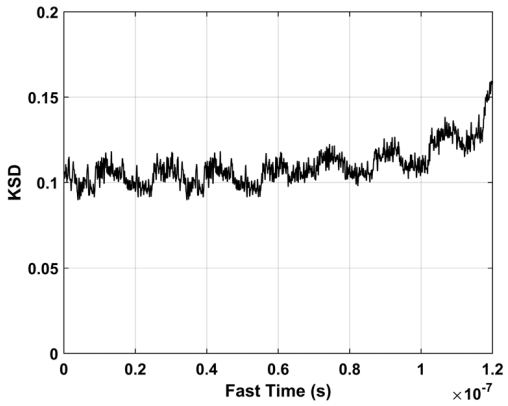

FIGURE 5. The KSD when a subject is not present.

To obtain a range estimate of the subject, an STFT [45] is applied on $\widehat{\Psi}$ which gives

$$K[o,p] = \sum_{m=1}^{M} \widehat{\Psi}[m,1]\,\Xi[o-m]\,e^{-j2p\pi m/P} \tag{37}$$

where P is the STFT window length which is equal to the number of fast time samples [45], and Ξ is the Hamming window given by

$$\Xi(o) = \alpha - \beta\cos\left(\frac{2\pi o}{O}\right), \quad o = 0, 1, \ldots, O \tag{38}$$

where $\alpha = 0.54$, $\beta = 0.46$, and $O = 512$ is the Hamming window width [46], [47].

The STFT output K without a subject is shown in Figure 6(a), and the corresponding output with a human subject is shown in Figure 6(b). These results indicate that the range can be estimated as

$$\widehat{L} = \frac{v\widehat{\tau}}{2} \tag{39}$$

where $\widehat{\tau}$ is the estimated propagation delay which corresponds to the maximum of K.

C. FREQUENCY ESTIMATION

Taking the FT of $\Phi(\tau, t)$ in each fast time dimension gives

$$Y(\upsilon, t) = a_v S(\upsilon)\, e^{-j2\pi\upsilon\tau_v(t)} \tag{40}$$

The index of the fast time estimate $\widehat{\tau}$ in $\Phi(\tau, t)$ is

$$\widehat{\Im} = \widehat{\tau}/\delta_T \tag{41}$$

and substituting this in $Y(\upsilon, t)$ gives

$$Y(\Im, t) = a_v S\left(\frac{\Im}{\delta_T}\right) e^{-j2\pi\frac{\Im}{\delta_T}\tau_v(t)} \tag{42}$$

which can be expressed as

$$Y(\Im, t) = a_v S\left(\frac{\Im}{\delta_T}\right)\cos\left[2\pi\frac{\Im}{\delta_T}\tau_v(t)\right] - ja_v S\left(\frac{\Im}{\delta_T}\right)\sin\left[2\pi\frac{\Im}{\delta_T}\tau_v(t)\right] \tag{43}$$

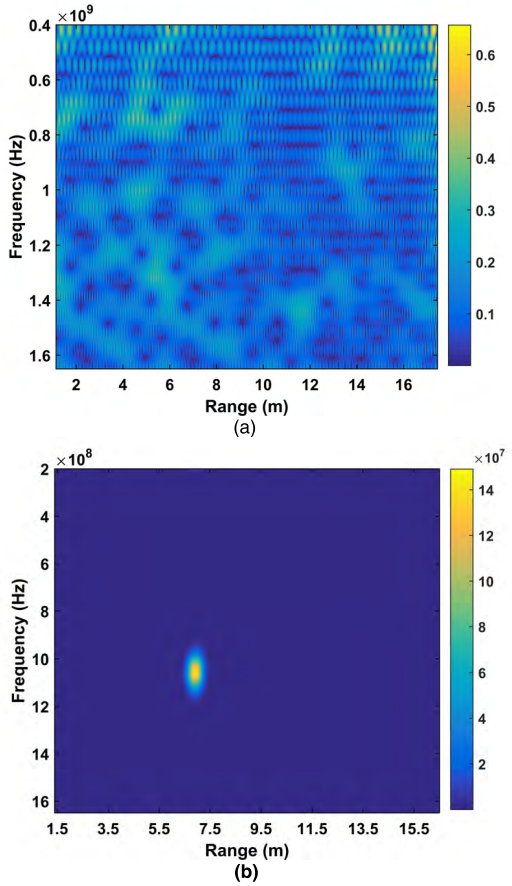

FIGURE 6. The STFT output (a) without a subject and (b) with a human subject.

Applying the AD method gives

$$\widehat{Y}(\Im, t) = \arctan \frac{M(\Im, t)}{N(\Im, t)} \tag{44}$$

where $N(\cdot)$ denotes the real part and $M(\cdot)$ denotes the imaginary part. The amplitude of the respiration signal can be obtained using (44). However, the effects of hardware inaccuracies and clutter can degrade this estimate. To improve the accuracy, the derivative of $M(\Im, t)/N(\Im, t)$ is used which is given by

$$\frac{d}{dt}\left[\frac{M(\Im, t)}{N(\Im, t)}\right] = \frac{N(\Im, t)[M(\Im, t)]' - [N(\Im, t)]' M(\Im, t)}{[M(\Im, t)]^2 + [N(\Im, t)]^2} \tag{45}$$

where $(M(\Im, t))'$ and $(N(\Im, t))'$ are the derivatives of $M(\Im, t)$ and $N(\Im, t)$, respectively. Integration is used to obtain $M(\Im, t)/N(\Im, t)$, and then the arctangent operation

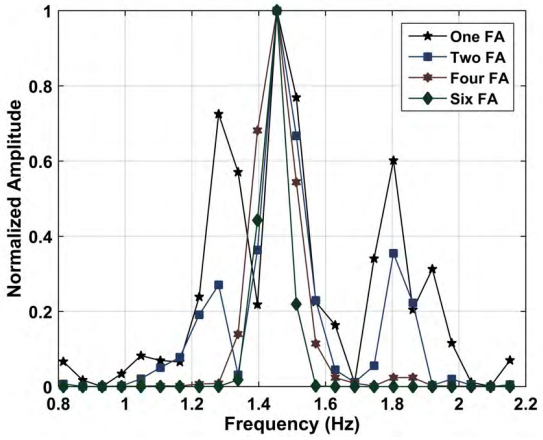

FIGURE 7. Clutter suppression using the multiple FA method.

is performed. The ideal vital sign signal is then

$$\overline{\overline{Y}}(t) = 2\pi \frac{\Im}{\delta_T} \tau_v(t) \tag{46}$$

and the corresponding result in discrete time is (47), as shown at the bottom of this page.

Based on prior knowledge of the vital sign signals, the respiration frequency is typically between 0.2 Hz and 0.5 Hz with an amplitude of 0.005 m to 0.015 m, and the heartbeat frequency is usually between 0.8 Hz and 2.5 Hz with an amplitude of 2 mm to 3 mm [23]. The SNCR can be improved by exploiting this information. In particular, components of the received signal outside these frequencies can be removed. A rectangular window χ is applied in the frequency domain which gives

$$\begin{aligned} \wp[n] &= \chi[n]\left\{\text{FFT}\left\{\overline{\overline{Y}}[n]\right\}\right\} \quad n \in K^*; \\ K^* &= k^*, k^*+1, \ldots, k^*+\kappa-1 \end{aligned} \tag{48}$$

where $\text{FFT}\left\{\overline{\overline{Y}}[n]\right\}$ is the FFT of $\overline{\overline{Y}}[n]$, and k^* is the index of the lowest frequency component to be retained.

To remove harmonics as well as the product of the respiration and heartbeat signals, a multiple FA method is employed which is based on the technique in [48] and is given by

$$\hbar[n] = |\ell[n] + j\ell[n]|^2 \tag{49}$$

$$\ell[n] = \begin{cases} 2\wp[n], & \kappa > 0 \\ 0, & \kappa < 0 \\ \wp[n], & \kappa = 0 \end{cases} \tag{50}$$

Figure 7 and Table 2 show the results obtained using this method. It can be seen that the unwanted signal components are suppressed when the FA method is applied, and increasing this number beyond four does not provide a significant

$$\overline{\overline{Y}}(n) = \sum_{k=2}^{n} \frac{N(\Im, k)[M(\Im, k) - M(\Im, k-1)] - M(\Im, k)[N(\Im, k) - N(\Im, k-1)]}{[M(\Im, k)]^2 + [N(\Im, k)]^2} \tag{47}$$

TABLE 2. Clutter suppression using the FA method.

Method	FFT	One FA	Two FA	Four FA	Six FA
SNR (dB)	-12.4	0.506	1.27	6.14	6.75

improvement. Thus, the FA method is used four times in the remainder of this paper.

IV. PERFORMANCE RESULTS AND DISCUSSION

A. DATA ACQUISITION

To validate the performance of the proposed method, several data sets were obtained using the UWB impulse radar in different conditions. In the experiments, the radar was placed on a table 1.3 m above ground. The transmit antenna was located on the top of the box, while the receive antenna was located on the bottom of the box. The wall is composed of three kinds of material, 0.30 m of brick, 0.35 m of concrete and 0.35 m of wood, which is similar to the ruins after a natural disaster. The subject stood behind the wall at different distances facing the radar while breathing normally.

The first experiment was conducted outdoors at the Institute of Electronics, Chinese Academy of Sciences in Beijing with the subject at distances of 3 m, 6 m, 9 m, and 11 m from the antenna as shown in Figure 8(a).

The second experiment was carried out indoors at the China National Fire Equipment Quality Supervision Center in Shanghai with distances between the antenna and subject of 4 m, 7 m, 10 m and 12 m as shown in Figure 8(b).

For the third experiment, an actuator was designed to imitate human vital sign signals. It moves at a frequency of 0.3333 Hz with an amplitude of 3 mm. The actuator was placed on a desk in the Shanghai indoor environment 1.3 m above ground at a distance between the antenna and actuator of 7 m, 10 m, and 12 m as shown in Figure 8 (c).

In the fourth experiment, the actuator was placed on a desk 1.5 m above ground outdoors in Beijing with a distance between the antenna and actuator of 9 m. The experimental data was analyzed using the FFT, CSD, CSD-AD, six FA-based CSD-AD, four FA-based CSD-AD, two FA-based CSD-AD, one FA-based CSD-AD, logarithm-based CSD (LCSD) and proposed methods. The results are presented below.

B. INITIAL PERFORMANCE

The performance with the steps before the FFT is discussed in this section using the outdoor experimental data for one female subject behind the wall facing the radar at a distance of 6 m from the antenna. The result after removing the clutter and linear trend is shown in Figure 9(a). This shows that the respiration signal is very weak and it is difficult to determine the oscillations. The results after filtering in fast and slow time are given in Figures 9(b) and 9(c), respectively, and

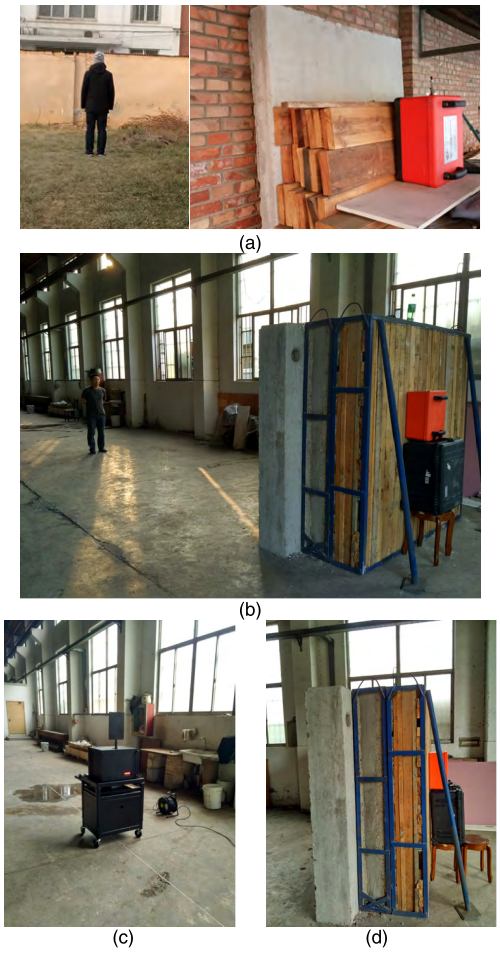

FIGURE 8. The experimental setup at the (a) Institute of Electronics, Chinese Academy of Sciences, (b) China National Fire Equipment Quality Supervision Center, and (c) China National Fire Equipment Quality Supervision Center with the actuator, and (d) the wall.

show that the vital sign signal is improved compared with Figure 9(a). However, the clutter between 1 s and 8 s cannot be removed, as it was introduced by a moving target in the detection environment. Figure 9(d) shows that using the SVD method reduces the effects of the clutter and thus enhances the respiration signal. These results indicate that the clutter caused by a moving target can be removed effectively using the SVD method.

C. PERFORMANCE WITH A HUMAN SUBJECT INDOORS

The datasets obtained with a human subject indoors at the China National Fire Equipment Quality Supervision Center in Shanghai are now considered. Assuming the desired signal is at a single frequency and all other signal components are noise and clutter, the SNR can be estimated as

$$SNR = 20\log_{10}\left(\frac{\sum_{n=\widehat{\Im}-1}^{\widehat{\Im}+1}|\hbar[\widehat{\tau},n]|}{\sum_{n=1}^{\widehat{\Im}-2}|\hbar[\widehat{\tau},n]|+\sum_{n=\widehat{\Im}+2}^{N}|\hbar[\widehat{\tau},n]|}\right) \quad (51)$$

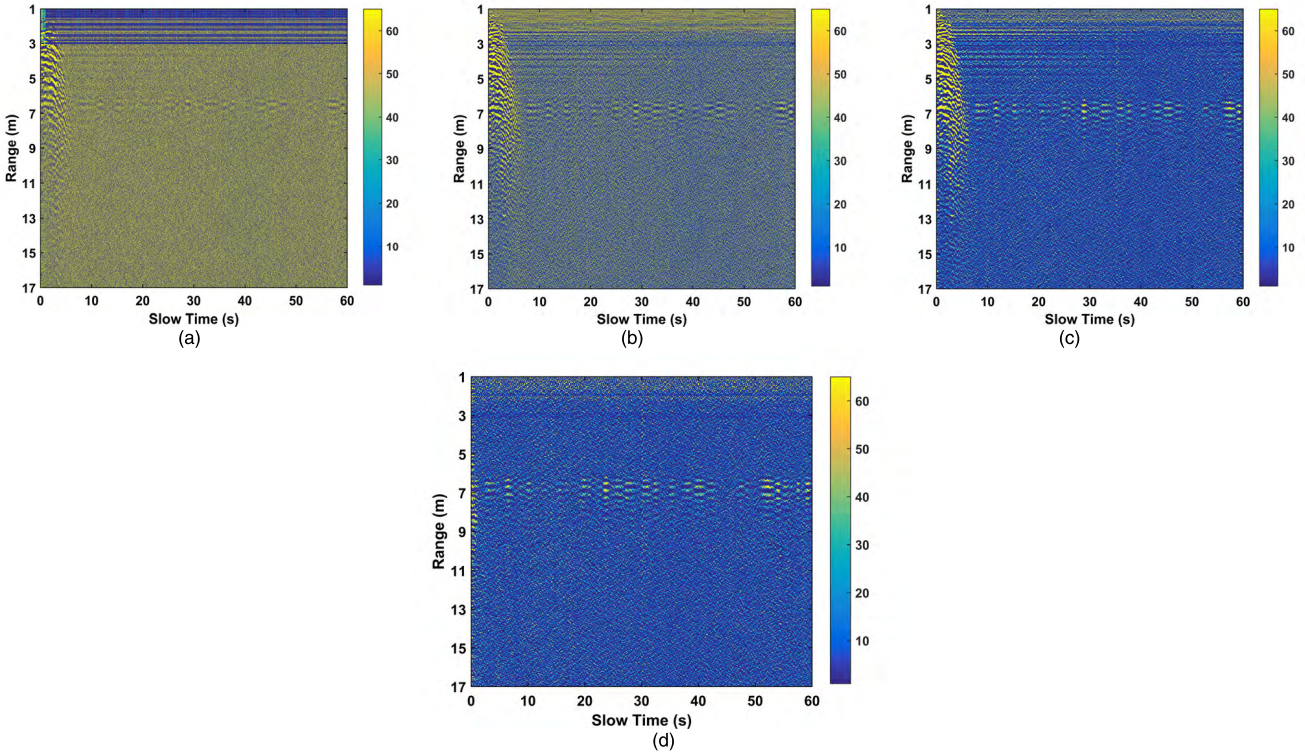

FIGURE 9. The results after (a) removing the static clutter and linear trend, (b) filtering in fast time, (c) filtering in slow time, and (d) SVD.

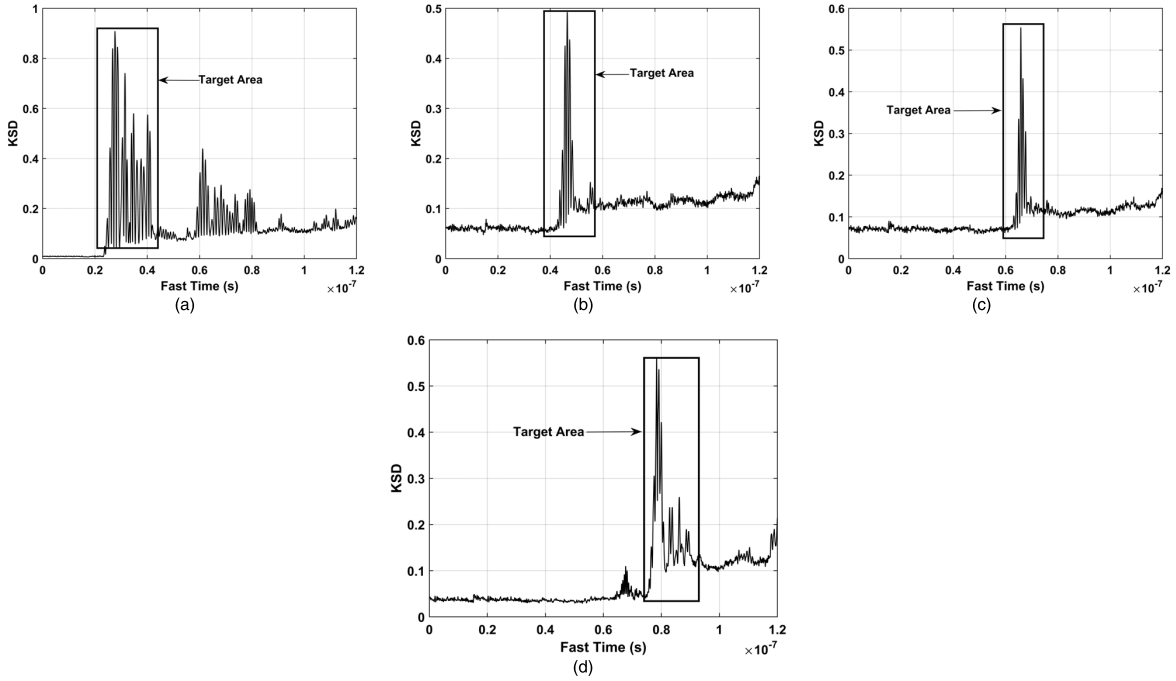

FIGURE 10. The standard deviation to kurtosis (KSD) for a human subject indoors at a distance from the antenna of (a) 4 m, (b) 7 m, (c) 10 m, and (d) 12 m.

The SNR will typically decrease as the detection distance increases [37]. Consequently, the improvement in SNR is considered for the data sets at each distance.

The KSD for several distances is given in Figure 10. This shows that the KSD varies significantly in the target area compared to the non-target area, and decreases with distance.

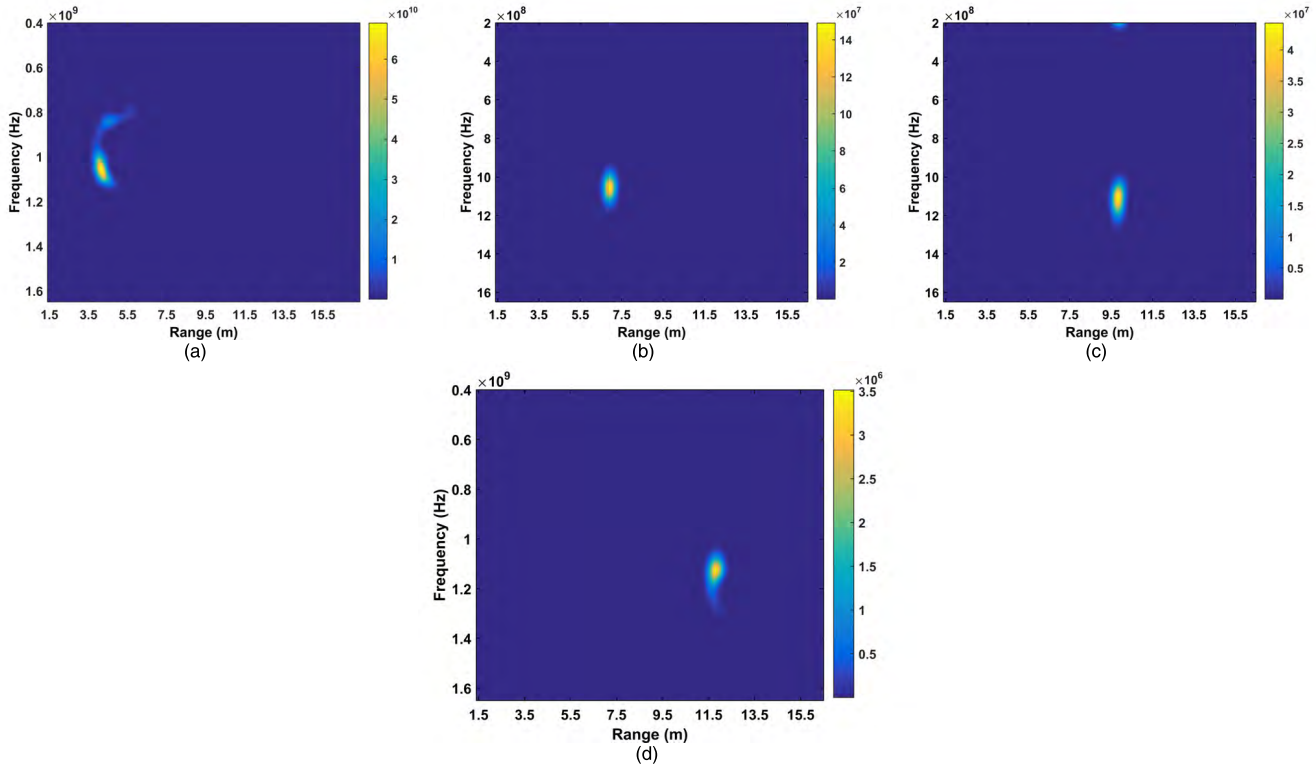

FIGURE 11. The estimated range obtained using the STFT technique at a distance from the antenna of (a) 4 m, (b) 7 m, (c) 10 m, and (d) 12 m.

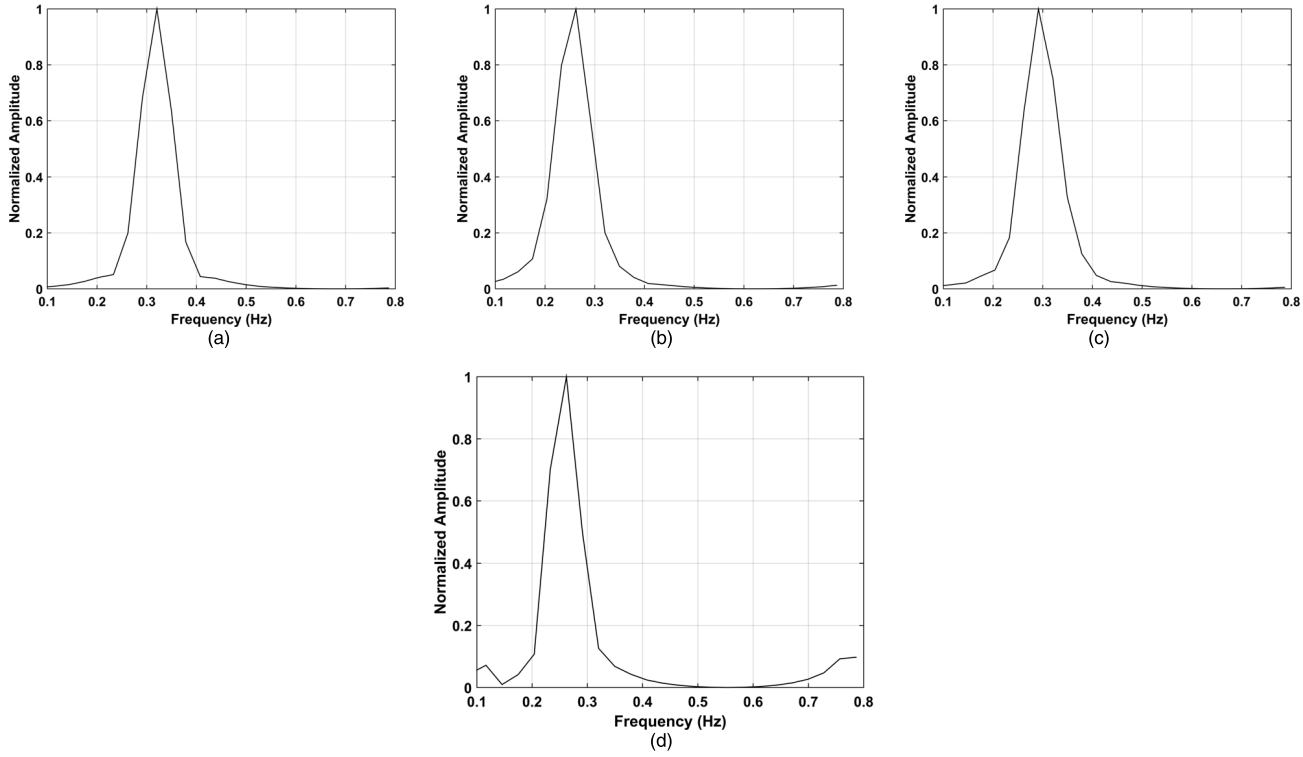

FIGURE 12. Respiration frequency estimation using the AD technique at a distance from the antenna of (a) 4 m, (b) 7 m, (c) 10 m, and (d) 12 m.

The estimated ranges obtained using the STFT technique are shown in Figure 11, and the corresponding respiration frequency estimates are given in Figure 12 and Table 3.

The errors in the range estimates with increasing distance are .104 m, .109 m, .109 m and .150 m, and the corresponding respiration frequency estimates are 0.32 Hz,

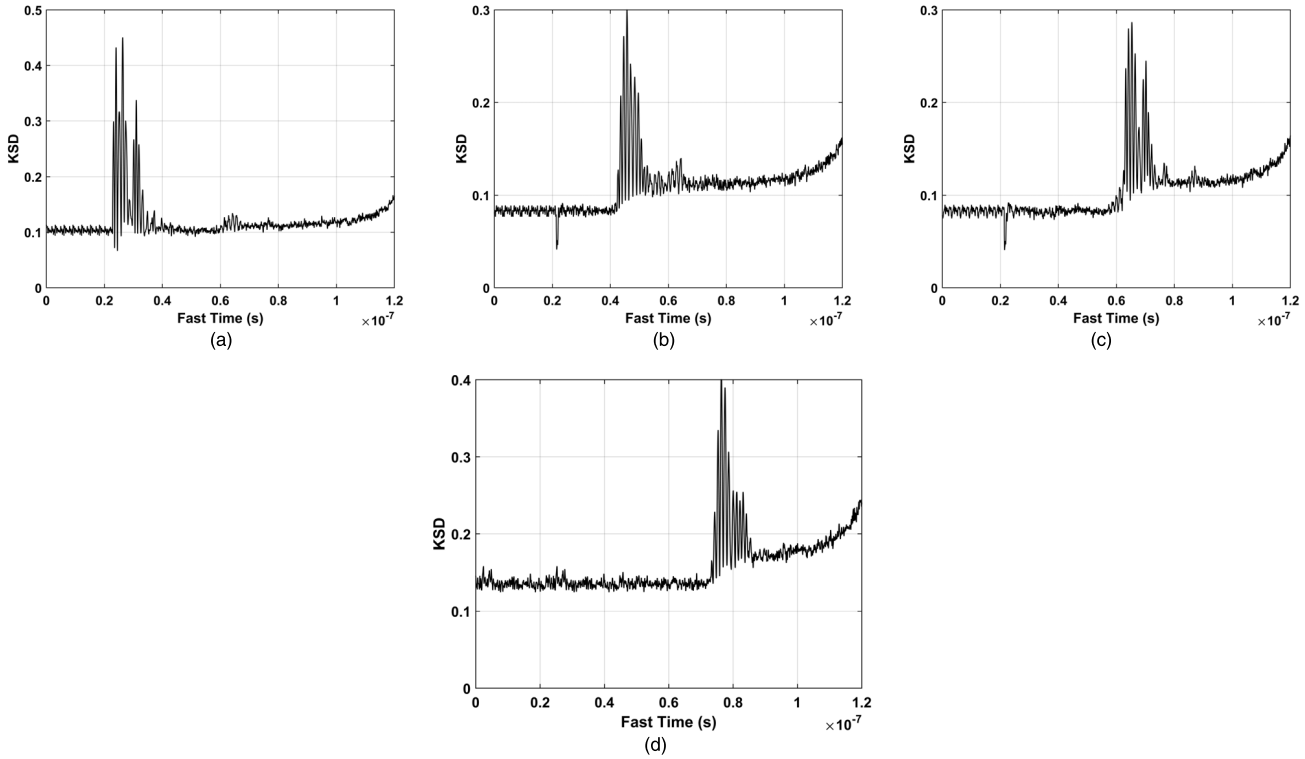

FIGURE 13. The KSD in the outdoor environment with a distance between the human subject and radar of (a) 3 m, (b) 6 m, (c) 9 m, and (d) 11 m.

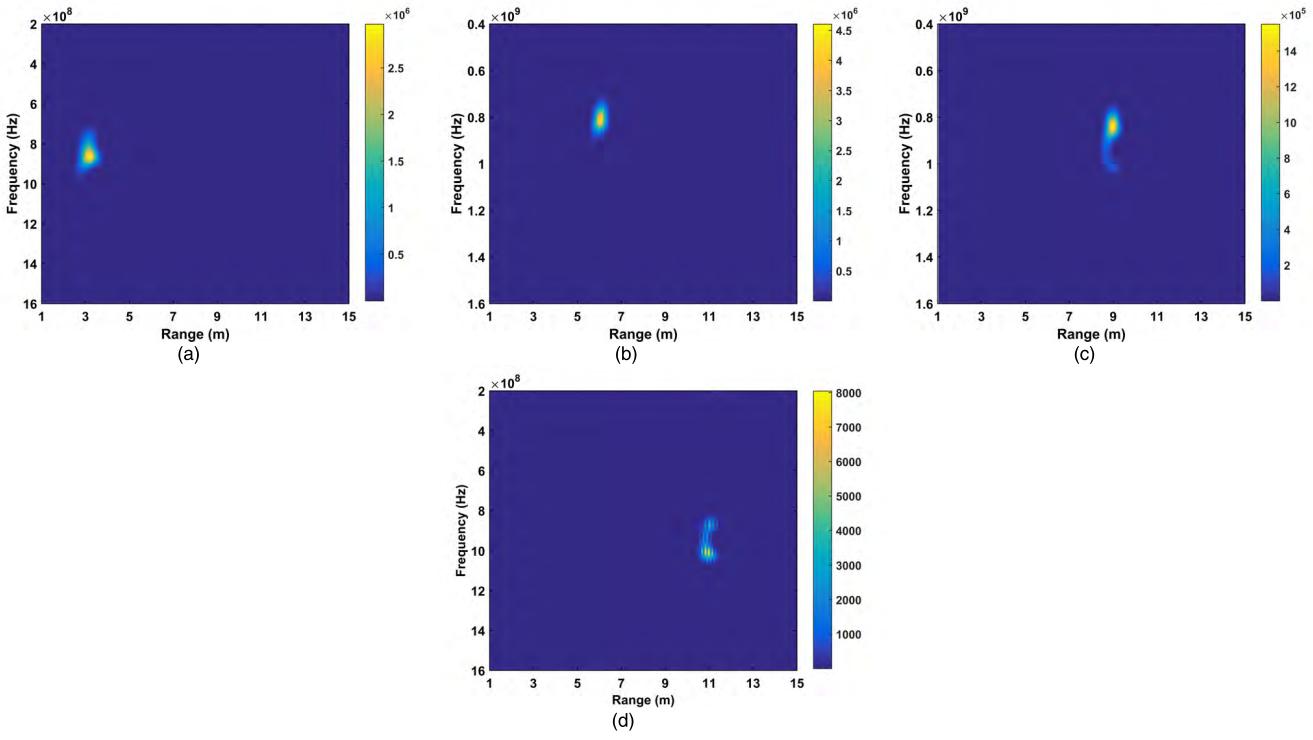

FIGURE 14. Range estimation with the proposed method in the outdoor environment with a distance between the subject and radar of (a) 3 m, (b) 6 m, (c) 9 m, and (d) 11 m.

0.26 Hz, 0.29 Hz, and 0.26 Hz, respectively. Table 3 also gives the estimates for the constant false alarm ratio (CFAR) method [32], advanced method (AM) [34], and multiple higher order cumulant (MHOC) method [35]. These results show that the proposed method provides superior performance as it results in the largest estimated SNRs.

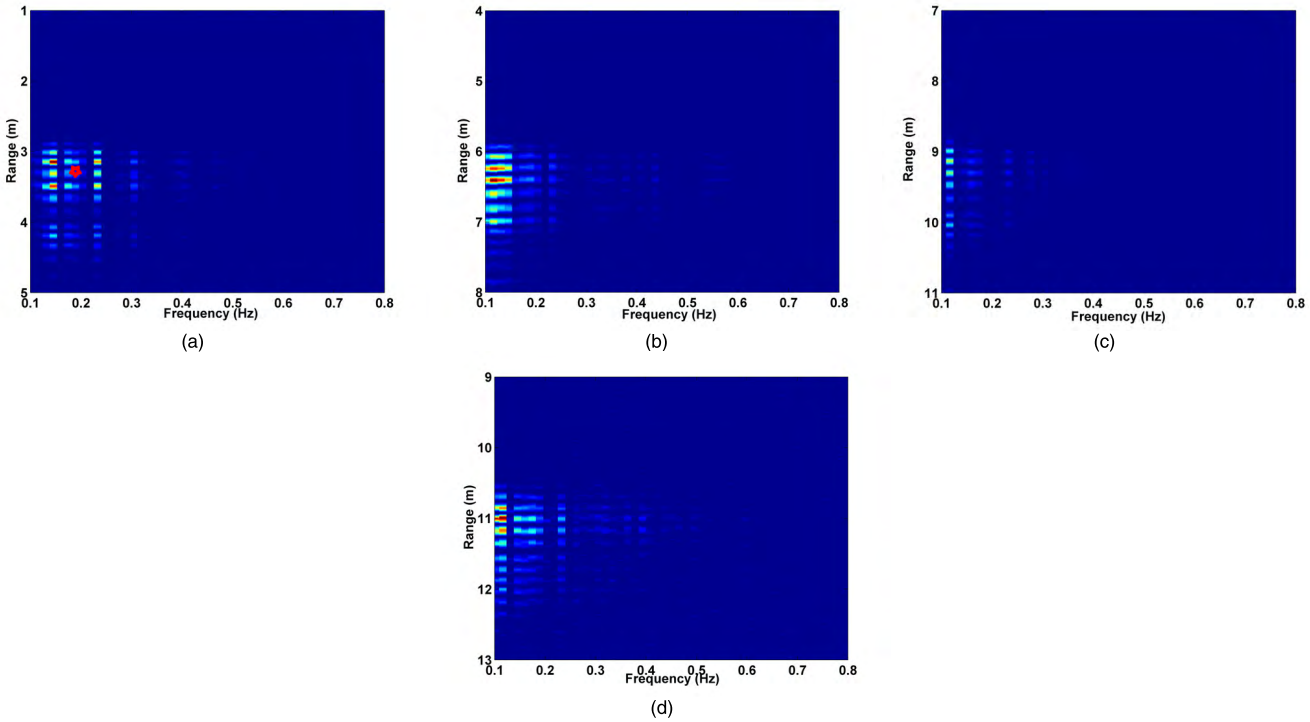

FIGURE 15. Range estimation using the CFAR method at a distance between the subject and radar of (a) 3 m, (b) 6 m, (c) 9 m, and (d) 11 m.

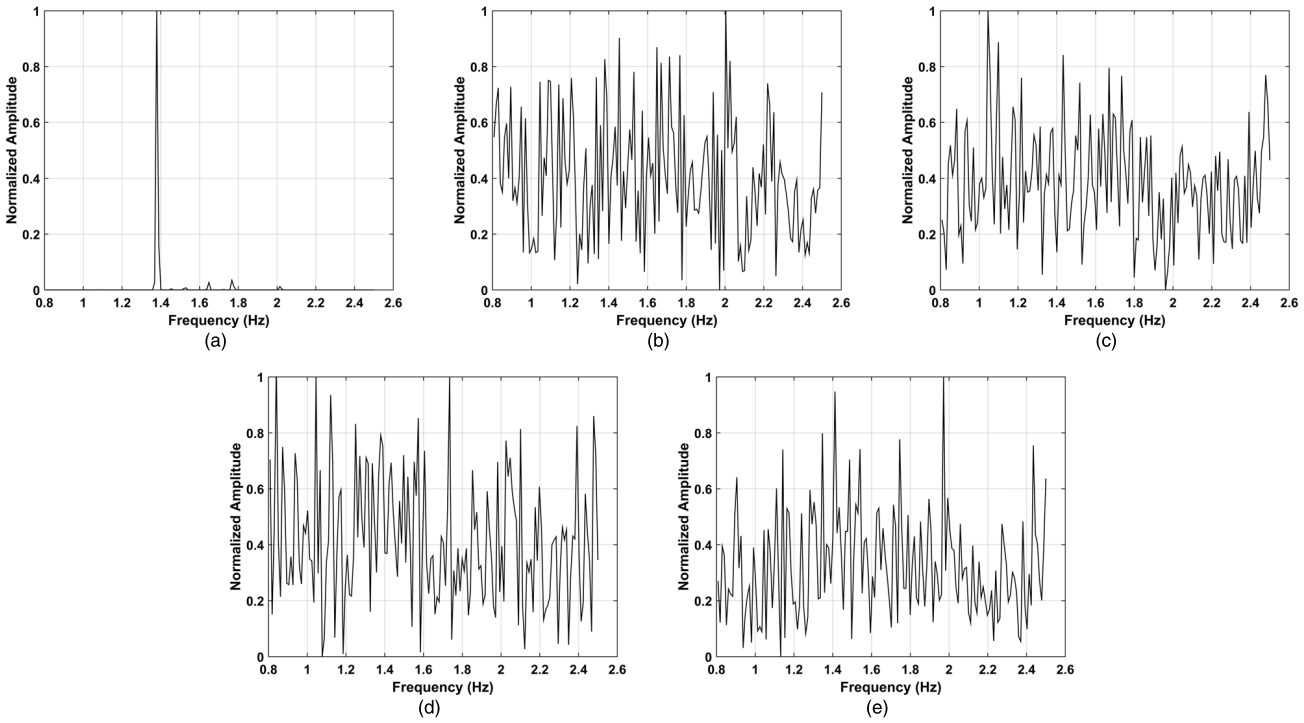

FIGURE 16. Heartbeat frequency estimation for the subject at a distance of 6 m from the antenna using the (a) proposed, (b) CSD-AD, (c) CSD, (d) logarithmic-based CSD, and (e) FFT methods.

D. PERFORMANCE WITH A HUMAN SUBJECT OUTDOORS

In this section, the datasets obtained for human subjects outdoors at the Institute of Electronics, Chinese Academy of Sciences are used to evaluate the performance. The CFAR method is used as a benchmark. The KSD using the proposed method is given in Figure 13. Figures 13(a) and 14(a) show the KSD and range estimates for the dataset with the subject 3 m from the antenna, Figures 13(b) and 14(b) show the

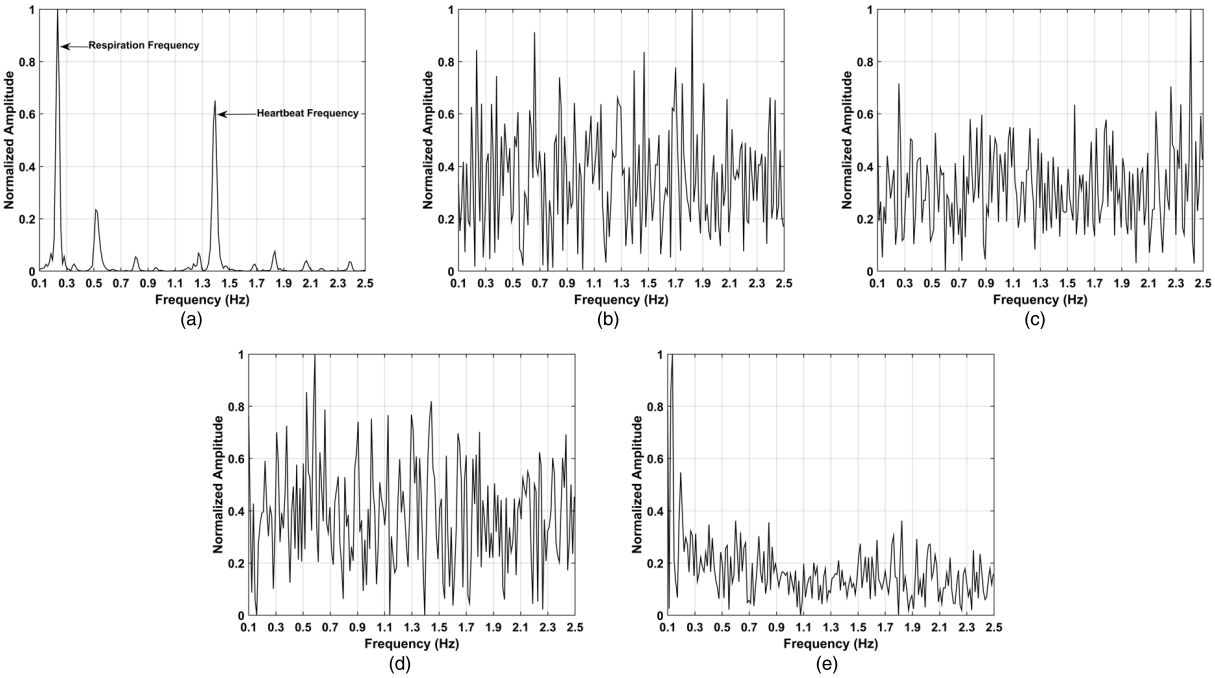

FIGURE 17. Frequency estimation results for the subject at a distance of 9 m from the radar antenna using the (a) proposed, (b) CSD-AD, (c) CSD, (d) logarithm-based CSD, and (e) FFT methods.

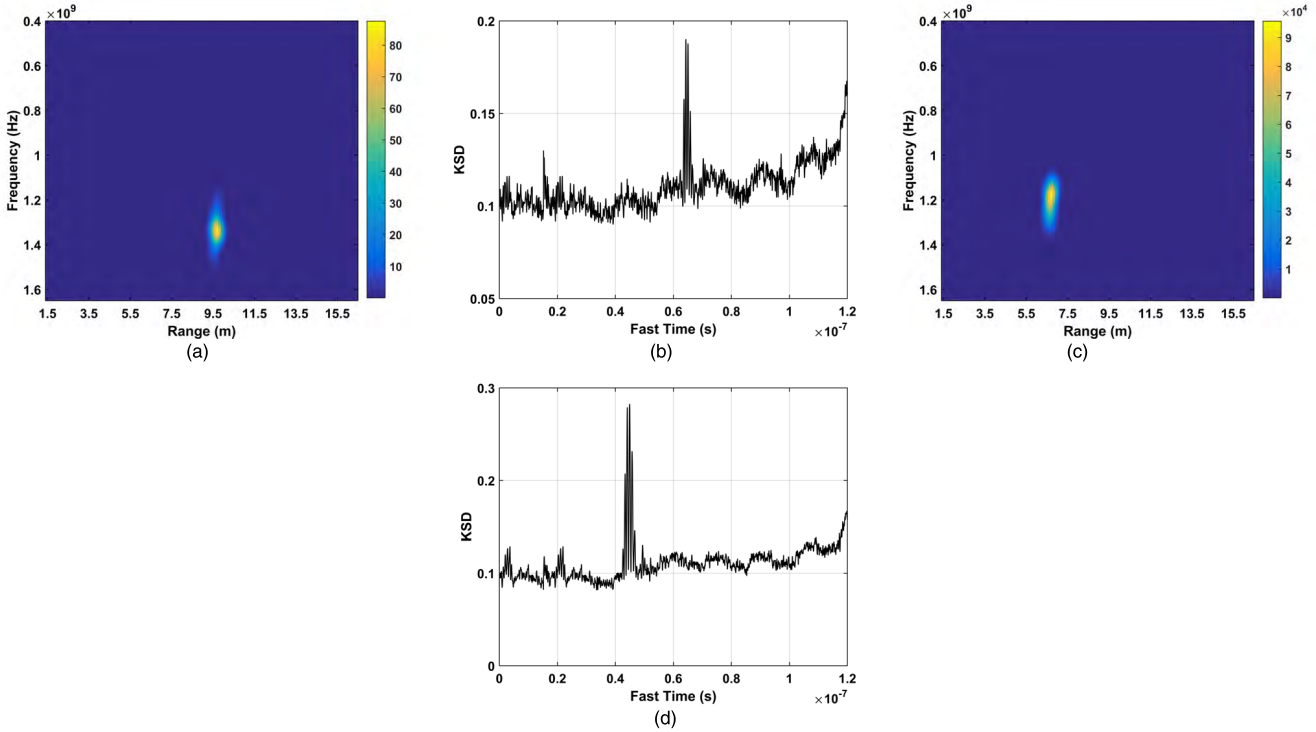

FIGURE 18. The performance of the actuator indoors (a) KSD with the actuator 10 m from the radar, (b) range estimate with the actuator 10 m from the radar, (c) KSD with the actuator 7 m from the radar, and (d) range estimate with the actuator 7 m from the radar.

corresponding results with the subject 6 m from the antenna, and Figures 13(c) and 14(c) and Figure 13(d) and 14(d) give the results for distances of 9 m and 11 m, respectively. The errors with increasing distance are .105 m, .254 m, .276 m and .302 m. These values are larger than the corresponding indoor errors due to the influence of wind. Fig. 15 shows the range estimation results using the CFAR method. The red star in Figure 15(a) indicates the estimated range

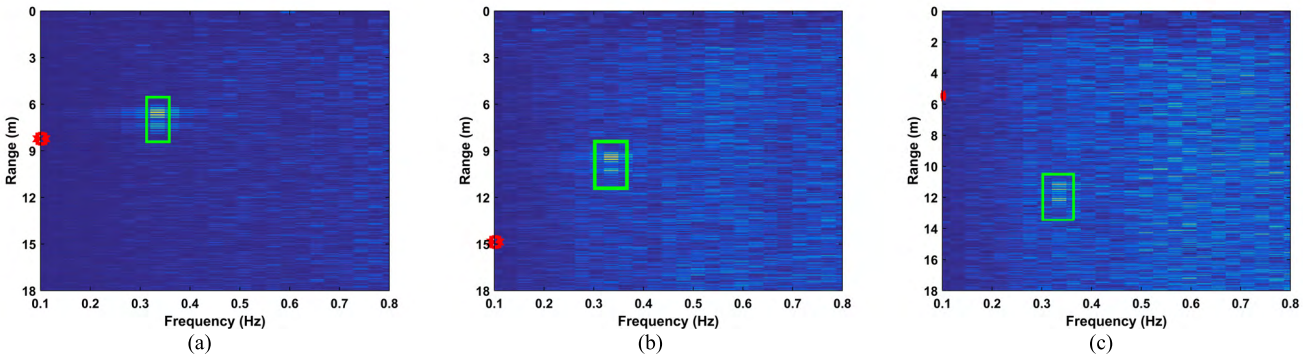

FIGURE 19. The performance with the AM method for a distance between the actuator and radar of (a) 7 m, (b) 10 m, and (c) 12 m.

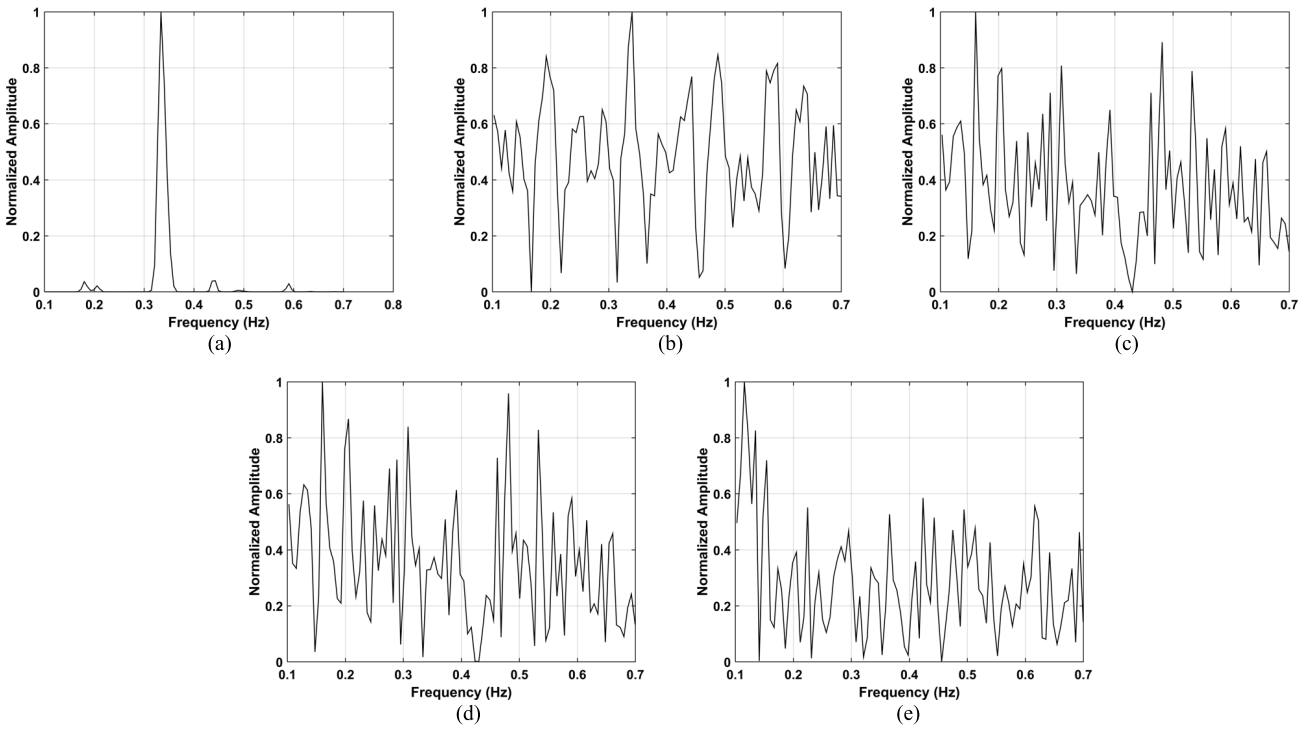

FIGURE 20. Actuator rate estimation indoors using the (a) proposed, (b) CSD-AD, (c) CSD, (d) logarithm-based CSD, and (e) FFT methods.

when the distance between the subject and antenna is 3 m. Figures 15(b) to 15(d) indicate that the range cannot be estimated for longer distances with this method. Thus, the proposed method outperforms the CFAR method especially when the human target is far from the radar.

The heartbeat frequency is estimated using the dataset for a distance between the antenna and subject of 6 m. The heart rate is usually 75 to 82 beats per minute i.e. a frequency of 1.25 Hz to 1.37 Hz. The normalized signal spectrums using different methods are shown in Figure 16, and the corresponding heart rate estimates are given in Table 4. The heartbeat frequency with the proposed method from Table 4 is 1.38 Hz. The CSD-AD and CSD methods provide heartbeat frequency estimates of 2.00 Hz and 1.05 Hz, as shown in Figures 16(b) and 16(c). Figures 16(d) and 16(e) give the results for the logarithm-based CSD and FFT methods, respectively. The frequency estimates are 0.84 Hz and 1.97 Hz. Thus, the proposed method gives the only normal estimate. Further, the proposed method provides the highest SNR.

The dataset obtained with the subject 9 m from the antenna is now analyzed. The results using the five methods are shown in Figure 17. Figure 17(a) indicates there are two peaks at 0.232 Hz and 1.39 Hz. Given the known signal characteristics, the first frequency corresponds to the respiration, while the second corresponds to the heartbeat. Harmonics and signal products are also present, but these are suppressed using the FA method. The results for the other four methods are given in Figures 17(b) to 17(e).

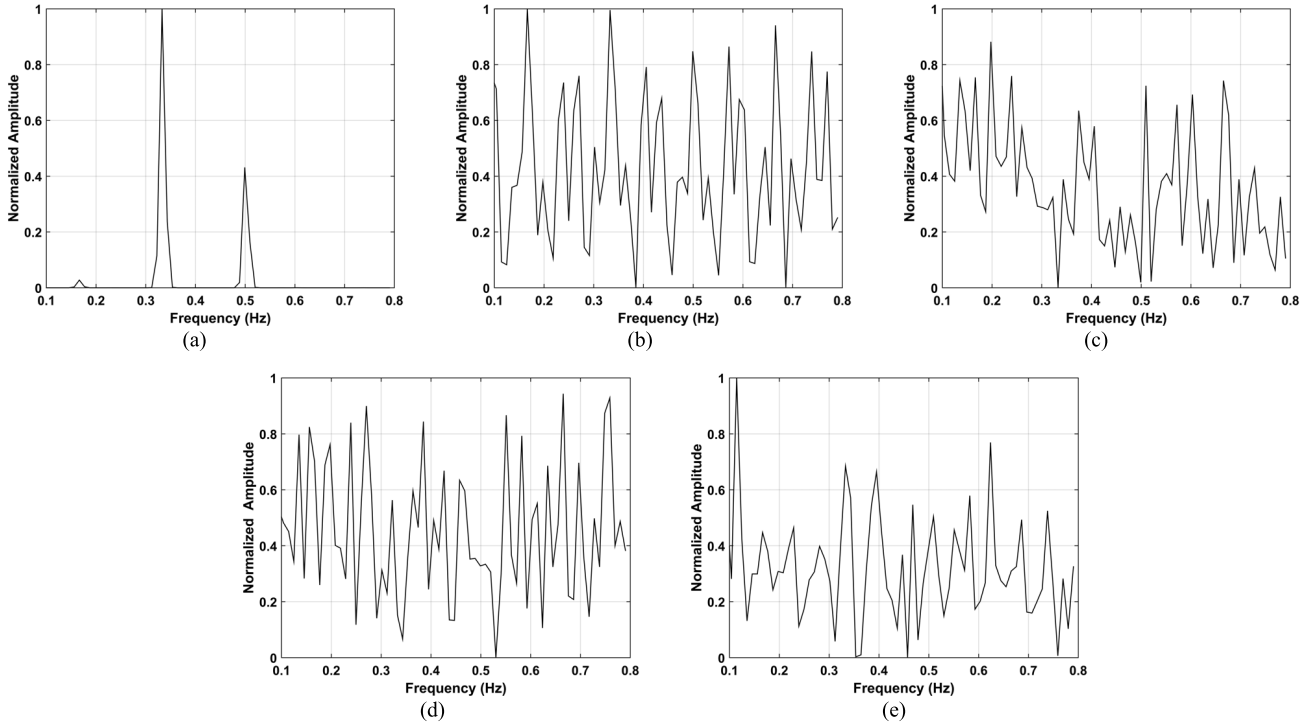

FIGURE 21. Estimation of the actuator rate outdoors using the (a) proposed, (b) CSD-AD, (c) CSD, (d) logarithmic-based CSD, and (e) FFT methods.

TABLE 3. Respiration frequency estimation performance with four different methods.

Method		4 m	7 m	10 m	12 m
CFAR	Error (m)	0.27	4.36	6.72	9.54
	Rate (Hz)	0.18	0.1	0.72	0.46
	SNR (dB)	-6.54	-8.22	-15.86	-17,26
Proposed	Error (m)	0.06	0.06	0.11	0.2
	Rate (Hz)	0.32	0.26	0.29	0.26
	SNR (dB)	6.58	3.52	3.27	1.35
MHOC	Error (m)	0.35	2.43	1.56	7.25
	Rate (Hz)	0.14	0.45	0.52	0.44
	SNR (dB)	-4.67	-6.85	-10.88	-12.78
AM	Error (m)	0.24	5.46	4.67	3.98
	Rate (Hz)	0.37	0.12	0.74	0.63
	SNR (dB)	3.35	-2.84	-6.69	-9.59

Comparing these results indicates that the proposed method provides the best performance.

E. ACTUATOR EXPERIMENT

In this section, the data obtained using the actuator is used to evaluate the performance of the proposed method. The actuator imitates human respiration motion with a frequency of 0.3333 Hz and an amplitude of 3 mm. The KSD and range estimates with the proposed method with the data obtained indoors at distances of 7 m and 10 m are shown in Figure 18. The range error is 0.208 m at a distance of 7 m. Figure 19 shows the results using the AM method, and indicates that both the range and the motion frequency cannot be estimated using this method. The corresponding signal spectrums are shown in Figure 20. The proposed method provides a motion rate estimate of 0.334 Hz as shown in Figure 20(a) with an error of only 0.001 Hz. Figure 20 and Table 5 indicate that the rate estimate is 0.340 Hz with the CSD-AD method, 0.161 Hz with the CSD method, 0.481 Hz with the logarithm CSD method, and 0.116 Hz with the FFT method. Table 5 also shows the SNR with these methods. These results indicate that the proposed method outperforms the other methods.

TABLE 4. Heartbeat frequency estimation results.

Method	Heartbeat Frequency (Hz)	SNR (dB)
FFT	1.97	-32.5
CSD-AD	2.00	-30.7
CSD	1.05	-32.1
Logarithm-based CSD	0.84	-28.6
Proposed	1.38	-20.6

The data obtained outdoors using the actuator at the Institute of Electronics, Chinese Academy of Sciences in Beijing

TABLE 5. Comparison of five motion rate estimation techniques.

Method	FFT	CSD-AD	CSD	Logarithmic-based CSD	Proposed
Motion Rate (Hz)	0.116	0.340	0.160	0.481	0.334
SNR (dB)	-31.1	-25.0	-32.8	-28.6	-12.1
Deviation (%)	65.4	2.04	51.9	44.4	0.120

is now considered. The motion rate estimation results for the five methods are shown in Figure 21. This indicates that the estimate for the proposed method is 0.3327 Hz with an error of only 0.0006 Hz. The estimate is 0.116 Hz with the CSD-AD method, 0.0934 Hz with the CSD method, 0.0832 Hz with the logarithm-based CSD method, and 0.114 Hz, with the FFT method. Thus, the proposed method is significantly better.

The results presented in this section show that vital sign information including the range and micro-motion frequency can be accurately estimated using the proposed method. Four experiments were conducted, two indoors and two outdoors, with a male subject and an actuator to simulate human respiration. The FFT, CSD, CSD-AD, six FA CSD-AD, four FA CSD-AD, two FA CSD-AD, one FA CSD-AD, logarithm-based CSD and proposed methods were investigated. The results obtained indicate that the static clutter, linear trend, harmonics, signal products, and other clutter in the same frequency band as the vital signs can be effectively suppressed using the proposed method. Further, both the range and motion frequency were accurately estimated.

V. CONCLUSION

In this paper, a new technique for vital sign detection was presented which employs a UWB impulse radar. The range of the subject was determined using a short-time Fourier transform (STFT), and the frequency of human motion was extracted using arctangent demodulation (AD) and a multiple frequency accumulation (FA) method. This information can be used to rescue trapped victims after natural disasters. The performance of this method was investigated using datasets obtained in different conditions and compared with several well-known techniques. Results were presented which indicate that the proposed approach can effectively suppress static and non-static clutter, linear trend, harmonics, and the product of respiration and heartbeat signals. Further, it can easily be implemented.

REFERENCES

[1] S. D. Liang, "Sense-through-wall human detection based on UWB radar sensors," *Signal Process*, vol. 126, pp. 117–124, Sep. 2016.
[2] M. Mercuri *et al.*, "Analysis of an indoor biomedical radar-based system for health monitoring," *IEEE Trans. Microw. Theory Techn.*, vol. 61, no. 5, pp. 2061–2068, May 2013.
[3] Y. Wan, Q. Si, Y. Lu, and X. Wang, "Ultra-wideband radar signals generated technology with two-channel," *Signal Process.*, vol. 87, no. 12, pp. 3101–3107, 2007.
[4] A. Singh *et al.*, "Data-based quadrature imbalance compensation for a CW doppler radar system," *IEEE Trans. Microw. Theory Techn.*, vol. 61, no. 4, pp. 1718–1724, Apr. 2013.
[5] L. Yang, W. Su, H. Gu, and R. Geng, "High-resolution velocity estimation and range profile analysis of moving target for pulse LFM UWB radar," *Signal Process.*, vol. 91, no. 10, pp. 2420–2425, 2011.
[6] Y. Nijsure *et al.*, "An impulse radio ultrawideband system for contactless noninvasive respiratory monitoring," *IEEE Trans. Biomed. Eng.*, vol. 60, no. 6, pp. 1509–1517, Jun. 2013.
[7] J. Li, L. Liu, Z. Zeng, and F. Liu, "Advanced signal processing for vital sign extraction with applications in UWB radar detection of trapped victims in complex environments," *IEEE J. Sel. Topics Appl. Earth Observ. Remote Sens.*, vol. 7, no. 3, pp. 783–791, Mar. 2014.
[8] Z. Li, W. Li, H. Lv, Y. Zhang, X. Jing, and J. Wang, "A novel method for respiration-like clutter cancellation in life detection by dual-frequency IR-UWB radar," *IEEE Trans. Microw. Theory Techn.*, vol. 61, no. 5, pp. 2086–2092, May 2013.
[9] W. Hu, Z. Zhao, Y. Wang, H. Zhang, and F. Lin, "Noncontact accurate measurement of cardiopulmonary activity using a compact quadrature Doppler radar sensor," *IEEE Trans. Biomed. Eng.*, vol. 61, no. 3, pp. 725–735, Mar. 2014.
[10] C. Gu and C. Li, "Assessment of human respiration patterns via noncontact sensing using doppler multi-radar system," *Sensors*, vol. 15, no. 3, pp. 6383–6398, 2015.
[11] A. Lazaro, D. Girbau, and R. Villarino, "Techniques for clutter suppression in the presence of body movements during the detection of respiratory activity through UWB radars," *Sensors*, vol. 14, no. 2, pp. 2595–2618, 2014.
[12] B. Yilmaz and C. Özdemir, "A detection and localization algorithm for moving targets behind walls based on one transmitter-two receiver configuration," *Microw. Opt. Technol. Lett.*, vol. 59, no. 6, pp. 1252–1259, 2017.
[13] L. Ren, Y. S. Koo, H. Wang, Y. Wang, Q. Liu, and A. E. Fathy, "Noncontact multiple heartbeats detection and subject localization using UWB impulse doppler radar," *IEEE Microw. Wireless Compon. Lett.*, vol. 25, no. 10, pp. 690–692, Oct. 2015.
[14] M.-C. Huang, J. J. Liu, W. Xu, C. Gu, C. Li, and M. Sarrafzadeh, "A self-calibrating radar sensor system for measuring vital signs," *IEEE Trans. Biomed. Circuits Syst.*, vol. 10, no. 2, pp. 352–363, Apr. 2016.
[15] F. JalaliBidgoli, S. Moghadami, and S. Ardalan, "A compact portable microwave life-detection device for finding survivors," *IEEE Embedded Syst. Lett.*, vol. 8, no. 1, pp. 10–13, Mar. 2016.
[16] G. Gennarelli, G. Ludeno, and F. Soldovieri, "Real-time through-wall situation awareness using a microwave Doppler radar sensor," *Remote Sens.*, vol. 8, no. 8, p. 621, 2016.
[17] C. Li *et al.*, "Searching for survivors through random human-body movement outdoors by continuous-wave radar array," *PLoS ONE*, vol. 11, no. 4, p. e0152201, 2016.
[18] C. Le, T. Dogaru, L. Nguyen, and M. A. Ressler, "Ultrawideband (UWB) radar imaging of building interior: Measurements and predictions," *IEEE Trans. Geosci. Remote Sens.*, vol. 47, no. 5, pp. 1409–1420, May 2009.
[19] Q. Huang, L. Qu, B. Wu, and G. Fang, "UWB through-wall imaging based on compressive sensing," *IEEE Trans. Geosci. Remote Sens.*, vol. 48, no. 3, pp. 1408–1415, Mar. 2010.
[20] V. T. Vu, T. K. Sjogren, M. I. Pettersson, A. Gustavsson, and L. M. H. Ulander, "Detection of moving targets by focusing in UWB SAR—Theory and experimental results," *IEEE Trans. Geosci. Remote Sens.*, vol. 48, no. 10, pp. 3799–3815, Oct. 2010.
[21] X. Zhuge and A. G. Yarovoy, "A sparse aperture MIMO-SAR-based UWB imaging system for concealed weapon detection," *IEEE Trans. Geosci. Remote Sens.*, vol. 49, no. 1, pp. 509–518, Jan. 2011.
[22] M. Ascione, A. Buonanno, M. D'Urso, L. Angrisani, and R. S. L. Moriello, "A new measurement method based on music algorithm for through-the-wall detection of life signs," *IEEE Trans. Instrum. Meas.*, vol. 62, no. 1, pp. 13–26, Jan. 2013.
[23] L. Liu, Z. Liu, and B. E. Barrowes, "Through-wall bio-radiolocation with UWB impulse radar: Observation, simulation and signal extraction," *IEEE J. Sel. Topics Appl. Earth Observ. Remote Sens.*, vol. 4, no. 4, pp. 791–798, Dec. 2011.
[24] L. Liu, Z. Liu, H. Xie, B. Barrowes, and A. C. Bagtzoglou, "Numerical simulation of UWB impulse radar vital sign detection at an earthquake disaster site," *Ad Hoc Netw.*, vol. 13, pp. 34–41, Feb. 2014.
[25] J. Wang, X. Wang, L. Chen, J. Huangfu, C. Li, and L. Ran, "Noncontact distance and amplitude-independent vibration measurement based on an extended DACM algorithm," *IEEE Trans. Instrum. Meas.*, vol. 63, no. 1, pp. 145–153, Jan. 2014.

[26] S. Xin, L. Biying, Z. Yang, Z. Lanzi, and Z. Zhimin, "Wall artifacts removal for target imaging enhancement in UWB through-the-wall radar application," *Signal Process.*, vol. 104, no. 6, pp. 325–338, 2014.
[27] E. Conte, A. Filippi, and S. Tomasin, "ML period estimation with application to vital sign monitoring," *IEEE Signal Process. Lett.*, vol. 17, no. 11, pp. 905–908, Nov. 2010.
[28] A. Nezirovic, A. G. Yarovoy, and L. P. Ligthart, "Signal processing for improved detection of trapped victims using UWB radar," *IEEE Trans. Geosci. Remote Sens.*, vol. 48, no. 4, pp. 2005–2014, Apr. 2010.
[29] H. Lv *et al.*, "Improved detection of human respiration using data fusion based on a multistatic UWB radar," *Remote Sens.*, vol. 8, no. 9, p. 773, 2016.
[30] Y. Wang, Q. Liu, and A. E. Fathy, "CW and pulse–Doppler radar processing based on FPGA for human sensing applications," *IEEE Trans. Geosci. Remote Sens.*, vol. 51, no. 5, pp. 3097–3107, May 2013.
[31] Z. Zhang, X. Zhang, H. Lv, G. Lu, X. Jing, and J. Wang, "Human-target detection and surrounding structure estimation under a simulated rubble via UWB radar," *IEEE Geosci. Remote Sens. Lett.*, vol. 10, no. 2, pp. 328–331, Mar. 2013.
[32] Y. Xu, S. Wu, C. Chen, J. Chen, and G. Fang, "A novel method for automatic detection of trapped victims by ultrawideband radar," *IEEE Trans. Geosci. Remote Sens.*, vol. 50, no. 8, pp. 3132–3142, Aug. 2012.
[33] Y. Xie and G. Fang, "Equi-amplitude tracing algorithm based on base-band pulse signal in vital sign detecting," *Electron. Inf. Technol.*, vol. 31, no. 5, pp. 1132–1135, 2009.
[34] S. Wu, K. Tan, Z. Xia, J. Chen, S. Meng, and F. Guangyou, "Improved human respiration detection method via ultra-wideband radar in through-wall or other similar conditions," *IET Radar, Sonar Navigat.*, vol. 10, no. 3, pp. 468–476, 2016.
[35] Y. Xu, S. Dai, S. Wu, J. Chen, and G. Fang, "Vital sign detection method based on multiple higher order cumulant for ultrawideband radar," *IEEE Trans. Geosci. Remote Sens.*, vol. 50, no. 4, pp. 1254–1265, Apr. 2012.
[36] X. Hu and T. Jin, "Short-range vital signs sensing based on EEMD and CWT using IR-UWB radar," *Sensors*, vol. 16, no. 12, p. 2025, 2016.
[37] C. Li and J. Lin, "Random body movement cancellation in Doppler radar vital sign detection," *IEEE Trans. Microw. Theory Techn.*, vol. 56, no. 12, pp. 3143–3152, Dec. 2008.
[38] B.-K. Park, O. Boric-Lubecke, and V. M. Lubecke, "Arctangent demodulation with DC offset compensation in quadrature Doppler radar receiver systems," *IEEE Trans. Microw. Theory Techn.*, vol. 55, no. 5, pp. 1073–1079, May 2007.
[39] K. Naishadham and J. E. Piou, "A robust state space model for the characterization of extended returns in radar target signatures," *IEEE Trans. Antennas Propag.*, vol. 56, no. 6, pp. 1742–1751, Jun. 2008.
[40] Z. Wu and N. E. Huang, "A study of the characteristics of white noise using the empirical mode decomposition method," *Proc. R. Soc. Lond. A, Math., Phys. Eng. Sci.*, vol. 460, no. 2046, pp. 1597–1611, 2004.
[41] Y. Yang and A. E. Fathy, "Development and implementation of a real-time see-through-wall radar system based on FPGA," *IEEE Trans. Geosci. Remote Sens.*, vol. 47, no. 5, pp. 1270–1280, May 2009.
[42] L. Liu and G. Fang, "A novel UWB sampling receiver and its applications for impulse GPR systems," *IEEE Geosci. Remote Sens. Lett.*, vol. 7, no. 4, pp. 690–693, Oct. 2010.
[43] J. Antoni, "The spectral kurtosis: A useful tool for characterising non-stationary signals," *Mech. Syst. Signal Process.*, vol. 20, no. 2, pp. 282–307, Feb. 2006.
[44] X. Liang, H. Zhang, T. Lu, and T. A. Gulliver, "Energy detector based TOA estimation for MMW systems using machine learning," *Telecommun. Syst.*, vol. 64, no. 2, pp. 417–427, 2017.
[45] R. Crochiere, "A weighted overlap-add method of short-time Fourier analysis/Synthesis," *IEEE Trans. Acoust., Speech, Signal Process.*, vol. 28, no. 1, pp. 99–102, Feb. 1980.
[46] J. B. Allen, "Short term spectral analysis, synthesis, and modification by discrete Fourier transform," *IEEE Trans. Acoust., Speech Signal Process.*, vol. 25, no. 3, pp. 235–238, Jun. 1977.
[47] K. Wojcicki, M. Milacic, A. Stark, J. Lyons, and K. Paliwal, "Exploiting conjugate symmetry of the short-time Fourier spectrum for speech enhancement," *IEEE Signal Process. Lett.*, vol. 15, pp. 461–464, 2008.
[48] L. Marple, "Computing the discrete-time 'analytic' signal via FFT," *IEEE Trans. Signal Process.*, vol. 47, no. 9, pp. 2600–2603, Sep. 1999.

XIAOLIN LIANG was born in Shandong, China, in 1988. He is currently pursuing the Ph.D. degree with the Department of Electronic Engineering, Ocean University of China, Qingdao, China. His research interests include ultra-wideband radio systems, 60-GHz wireless systems, signal processing, UWB radar, and vital sign detection.

HAO ZHANG (SM'13) was born in Jiangsu, China, in 1975. He received the B.S. degree in telecom engineering and industrial management from Shanghai Jiaotong University, China, in 1994, the M.B.A. degree from the New York Institute of Technology, New York, NY, USA, in 2001, and the Ph.D. degree in electrical engineering from the University of Victoria, Victoria, BC, Canada, in 2004. From 1994 to 1997, he was an Assistant President of ICO (China) Global Communications Company. He is currently a Professor with the Department of Electrical Engineering, Ocean University of China. He is also an Adjunct Professor with the University of Victoria. His research interests include ultra-wideband systems, MIMO wireless systems, and spread spectrum communications.

GUANGYOU FANG received the B.S. degree in electrical engineering from Hunan University, Changsha, China, in 1984, and the M.S. and Ph.D. degrees in electrical engineering from Xi'an Jiaotong University, Xi'an, China, in 1990 and 1996, respectively. From 1990 to 1999, he was an Engineer, an Associate Professor, and a Professor with the China Research Institute of Radiowave Propagation, Xinxiang, China. From 2000 to 2001, he was a Visiting Scholar with the University of Trieste, Trieste, Italy, and the International Center for Science and High Technology-United Nations Industrial Development Organization, Trieste. From 2001 to 2003, he was a Special Foreign Research Fellow of the Japan Society for the Promotion of Science with Tohoku University, Sendai, Japan. Since 2004, he has been a Professor with the Institute of Electronics, Chinese Academy of Sciences, Beijing, China, and the Director of the Key Laboratory of Electromagnetic Radiation and Sensing Technology. He is the author of over 100 publications. His research interests include UWB radar, ground-penetrating radar signal processing and identification methods, and computational electromagnetics.

SHENGBO YE received the Ph.D. degree from the Institute of Electronics, Chinese Academy of Sciences (CAS), Beijing, China, in 2011. Since 2011, he has been with the Key Laboratory of Electromagnetic Radiation and Sensing Technology, CAS. His research interests include UWB through-wall radar detection, imaging, ground-penetrating radar signal processing life detection, and other related applications.

T. AARON GULLIVER (SM'96) received the Ph.D. degree in electrical engineering from the University of Victoria, Victoria, BC, Canada, in 1989. From 1989 to 1991, he was a Defence Scientist with the Defence Research Establishment Ottawa, Ottawa, ON, Canada. He has held academic positions at Carleton University, Ottawa, and the University of Canterbury, Christchurch, New Zealand. He joined the University of Victoria in 1999 and is a Professor with the Department of Electrical and Computer Engineering. He is a member of the Association of Professional Engineers of Ontario, Canada. His research interests include information theory and communication theory, algebraic coding theory, cryptography, construction of optimal codes, iterative coding, MIMO communications, space-time coding, and ultra-wideband communications. In 2002, he became a fellow of the Engineering Institute of Canada, and in 2012 a fellow of the Canadian Academy of Engineering.